SCIENCE CHINA
Physics, Mechanics & Astronomy

• Article •

October 2017 Vol. 60 No. 10: 106111
doi: 10.1007/s11433-017-9051-6

Development of soft magnetic amorphous alloys with distinctly high Fe content

PingBo Chen[1,2,3], AnDing Wang[1,4*], ChengLiang Zhao[1,2], AiNa He[1,2], Gang Wang[3], ChunTao Chang[1,2*], XinMin Wang[1,2], and Chain-Tsuan Liu[4]

[1] *Key Laboratory of Magnetic Materials and Devices, Ningbo Institute of Materials Technology and Engineering, Chinese Academy of Sciences, Ningbo 315201, China;*
[2] *Zhejiang Province Key Laboratory of Magnetic Materials and Application Technology, Ningbo Institute of Materials Technology and Engineering, Chinese Academy of Sciences, Ningbo 315201, China;*
[3] *Laboratory for Microstructures, Institute of Materials Science, Shanghai University, Shanghai 200444, China;*
[4] *Center for Advanced Structural Materials, Department of Mechanical and Biomedical Engineering, College of Science and Engineering, City University of Hong Kong, Hong Kong 999077, China*

Received March 29, 2017; accepted May 8, 2017; published online August 11, 2017

This paper reports on the preparation of $Fe_{82.7\text{-}85.7}Si_{2\text{-}4.9}B_{9.2\text{-}11.2}P_{1.5\text{-}2.7}C_{0.8}$ soft magnetic amorphous alloys with a distinctly high Fe content of 93.5-95.5 wt.% by component design and composition adjustment. All alloys can be readily fabricated into completely amorphous ribbon samples with good surface quality by the single copper roller melt-spinning method. These alloys show good bending ductility and excellent magnetic properties after annealing, i.e., low coercivity (H_c) of 3.3-5.9 A/m, high permeability (μ_e) of 5000-10000 and high flux saturation density (B_s) of 1.63-1.66 T. The mechanism of the good glass forming ability (GFA) and soft-magnetic properties are explored. The amorphous alloys with the high Fe content comparable to that of the desired high Si alloy can be promising candidates for the potential application in electric devices.

metallic glasses, alloy design, annealing, magnetic properties, shear band

PACS number(s): 02.30.Sa, 05.70.Fh, 05.30.Rt, 64.70.Tg, 05.20.Dd

Citation: P. B. Chen, A. D. Wang, C. L. Zhao, A. N. He, G. Wang, C. T. Chang, X. M. Wang, and C. T. Liu, Development of soft magnetic amorphous alloys with distinctly high Fe content, Sci. China-Phys. Mech. Astron. **60**, 106111 (2017), doi: 10.1007/s11433-017-9051-6

1 Introduction

Since Si steels with good magnetic properties were found by Hadfield in 1900, electric steels have been widely used in the electric and magnetic fields [1]. During the subsequent research, it is found that the magnetic anisotropy (K_1) and magnetostriction coefficient (λ_s) decrease with the increase of Si content [2], all of which will lead to the improvement of soft magnetic properties and frequency characteristics [3]. However, when the Si content exceeds 4 wt.%, the workability of the Si steels is dramatically reduced, making it extremely difficult to produce high Si steel sheet by the common hot-cold rolling process [4]. To solve this problem, a variety of experiments have been conducted over the years using rolling, rapid quenching, and chemical vapor deposition (CVD) siliconizing methods in an attempt to produce high Si steel sheet [5-7]. Nevertheless, the mass production of high Si steel (>4.5 wt.% Si) is still unsatisfactory as indicated in Figure 1(a) [8].

As a new generation electric material, amorphous alloys have been proved to exhibit better soft magnetic properties,

*Corresponding authors (AnDing Wang, email: anding@nimte.ac.cn; ChunTao Chang, email: ctchang@nimte.ac.cn)

© Science China Press and Springer-Verlag Berlin Heidelberg 2017

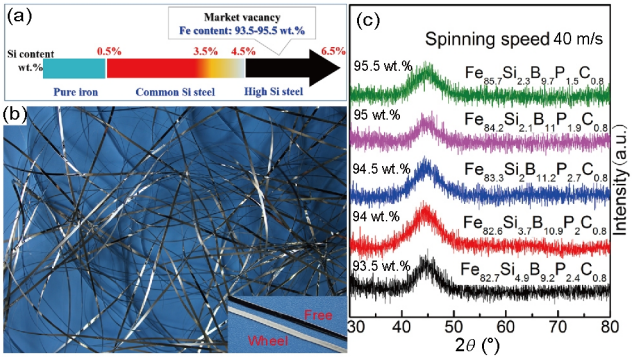

Figure 1 (Color online) (a) Research requirement of electric alloy; (b) pictures of the as spun ribbons; (c) XRD patterns of the soft magnetic amorphous alloys with different Fe content.

higher electric resistivity, lower core loss and anticorrosion owing to the amorphous structure [9], which are considered as good complementary products and even replacers. The production line for the rapid quenching method of the amorphous alloys is also shorter than that of the traditional rolling process of the Si alloys [4], and this will result in a significant reduction of the production energy, time consumed and cost. However, due to the limited GFA of the alloys, a considerable amount of amorphous forming elements are added in the previously developed amorphous alloys, which inevitably leads to a low Fe content and B_s [10-12]. Therefore, it is vitally important to develop a high Fe content amorphous soft magnetic alloy for soft magnetic applications [13].

In our recent work, a method for developing high B_s amorphous alloys was devised in base of composition designing. We developed a new resulting FeSiBPC amorphous alloy system with good magnetic properties and manufacturability [14]. Due to the small atomic number of amorphous forming elements, it is promising to fabricate the high Fe content alloys as compared with traditional electric alloys. In this study, $Fe_{82.7\text{-}85.7}Si_{2\text{-}4.9}B_{9.2\text{-}11.2}P_{1.5\text{-}2.7}C_{0.8}$ soft magnetic amorphous alloys with a distinctly high Fe content of 93.5-95.5 wt.% were designed by further adjusting metal elements and the ratios of metalloid elements. The mechanism controlling their good GFA and soft-magnetic properties are explored. These amorphous alloys with a higher Fe content comparable to that of the desired high Si alloy are promising candidates for potential applications in electric and magnetic devices.

2 Experiment procedure

Multicomponent alloys with nominal atomic compositions of $Fe_{82.7}Si_{4.9}B_{9.2}P_{2.4}C_{0.8}$ (Fe-93.5 wt.%), $Fe_{82.6}Si_{3.7}B_{10.9}P_2C_{0.8}$ (Fe-94 wt.%), $Fe_{83.3}Si_2B_{11.2}P_{2.7}C_{0.8}$ (Fe-94.5 wt.%), $Fe_{84.2}Si_{2.1}B_{11}P_{1.9}C_{0.8}$ (Fe-95 wt.%), and $Fe_{85.7}Si_{2.3}B_{9.7}P_{1.5}C_{0.8}$ (Fe-95.5 wt.%) were designed. We prepared the master alloys by induction-melting the mixture of Fe (99.99 wt.%), crystal B (99.5 wt.%), Si (99.999 wt.%) and pre-alloyed Fe_3P and Fe-3.6%C ingots in an argon atmosphere. Ribbons with a width of about 1 mm and thickness of about 23-26 μm were fabricated by single roller melt-spinning method. The amorphous structure was identified by X-ray diffraction (XRD) with Cu kα radiation. Thermal parameters including Curie temperature (T_c) and crystallization temperature (T_x) of the amorphous alloys were examined by differential scanning calorimetry (DSC) at a heating rate of 40°C/min. The solidification temperature (T_{ls}) was measured with DSC by cooling the molten master alloy samples at a low cooling rate of 4°C/min. As the magnetic properties depend on the sample sizes, ribbon samples with similar sizes mentioned above were used for measurement to clarify the intrinsic soft-magnetic properties of this glassy alloy system. Before measuring the magnetic properties, the ribbon samples were annealed from 260°C to 400°C for 10 min in order to reduce the influence of the stress by structure release. H_c was recorded with a DC *B-H* loop tracer under a field of 800 A/m, μ_e at 1 kHz with an impedance analyzer under a field of 1 A/m, and B_s by vibrating sample magnetometer (VSM) with a maximum applied field of 800 kA/m. The mass of samples was measured by using an electronic balance (Mettler XS105DU, Switzerland), with high accuracy of ±0.00001 g and the density of the master alloys was obtained by Archimedes method. All mass and density values were averaged by multiple tests in order to ensure the accuracy. In order to eliminate the influence of demagnetizing factors on soft-magnetic properties, the lengths of the samples for DC *B-H* loop tracer and impedance analyze measurement were 75 mm, much larger than the width and thickness. The structure of magnetic domain was characterized via the Magneto-optical Kerr Microscope (4-873K/950MT, Germany). The bent region of the amorphous samples were examined by scanning electron microscopy (SEM). All the measurements were carried out at room temperature.

3 Results and discussion

The compositions of high Fe-content soft magnetic amorphous alloys were designed by adjusting the metalloid elements of Si, B and P [14]. The soft magnetic amorphous alloys exhibit the distinctly high Fe content of 93.5-95.5 wt.% in comparison with the Fe content in the high Si alloys. As the alloys are close to the upper limit of the Fe content for forming a fully amorphous state by using common melt spun progress, composition adjustment was repeatedly done in different series. As shown in Figure 1(b), all of the alloys can be readily fabricated into ribbon samples with good surface quality and ductility by single roller melt-spinning method. Compared with the brittle nature, severe fabricating process and poor surface quality of high Si content steel, these alloys enjoy much better manufacturability which is crucial for mass

production and application. XRD pattern shows broad peaks without appreciable crystalline peaks (Figure 1(c)), which is a good support of the amorphous structure.

Figure 2(a) shows DSC curves of the melt-spun high Fe content amorphous alloys. All curves have two distinctly separated exothermic peaks, corresponding to the two stages of crystallization process. According to the previous study, the first and second peaks are correlated to the precipitation of α-Fe and compound phases [15], respectively. With the rise of Fe content, the onset of crystallization temperature (T_{x1}) declined drastically from 463°C to 389°C, implying the easier formation of α-Fe cluster, which may augment the B_s during annealing. For the alloys with high Fe content, the hindering effect of metalloid elements weakened, which will lead to a high diffusion rate and a lower crystallization energy. As enlarged in Figure 2(a), an endothermic peak can be observed in every curve before the first exothermic peak, which has been proved to be the result of Curie transition from ferromagnetic state to paramagnetic state [16]. Compared with the commercial $Fe_{78}Si_9B_{13}$ (393°C) and $Fe_{82}Si_4B_{13}C_1$ (355°C) alloys, the T_c in the range of 266°C-336°C turned to be comparatively lower, indicating a lower annealing temperature which is beneficial for decreasing the brittleness of annealed ribbons [17]. It has been well accepted that T_c and T_{x1} are important factors for determining the annealing temperature (T_A) [18]. In order to get excellent soft magnetic properties, the temperature between T_c and T_{x1} is chosen to release inner stresses without crystallization. The T_{x1}-T_c values are all about 120°C, similar to those of the commonly used $Fe_{78}Si_9B_{13}$ and $Fe_{82}Si_4B_{13}C_1$ amorphous alloys [18]. DSC curves in Figure 2(b) show the solidification behavior of the master alloys. As the solidification process is quasi-static because of the low cooling rate, T_{ls} reflects the liquidus temperature and undercooling. The current amorphous alloys exhibit a lower T_{ls} compared with $Fe_{78}Si_9B_{13}$ and $Fe_{82}Si_4B_{13}C_1$ alloys [19]. After the first solidification event, a sharp peak is observed for every alloy, which always originates form the synchronously precipitation of the phases. In fast cooling processes, the competing effect has been proved to be important for inhibiting crystallization [20]. During our composition exploration process, we failed to adjust the two peaks to a single peak for high Fe content alloys. Taking all these conditions into account, the current amorphous alloys with a larger T_{x1}-T_c and a lower T_{ls} are expected to exhibit good amorphous-forming ability and excellent soft-magnetic properties.

Variations of H_c for amorphous soft magnetic alloys as a function of T_A are presented in Figure 3(a). The H_c decreases slightly with the increase of T_A until reaching the lowest value, which can be attributed to the stress releasing. For most alloys, the lowest H_c is only about 3-5 A/m, except for the $Fe_{85.7}Si_{2.3}B_{9.7}P_{1.5}C_{0.8}$ ribbon sample showing the lowest H_c of 5.9 A/m. Changes of μ_e as a function of T_A are shown in Figure 3(b). It is clear that the μ_e of these soft magnetic

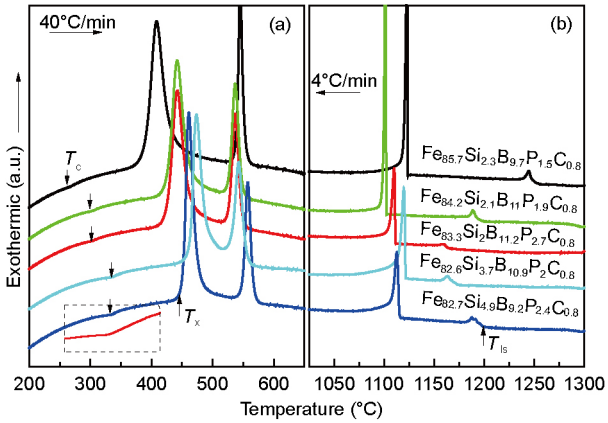

Figure 2 (Color online) (a) DSC curves of the high Fe content amorphous ribbons; (b) DSC curves of the master alloy showing the solidification process.

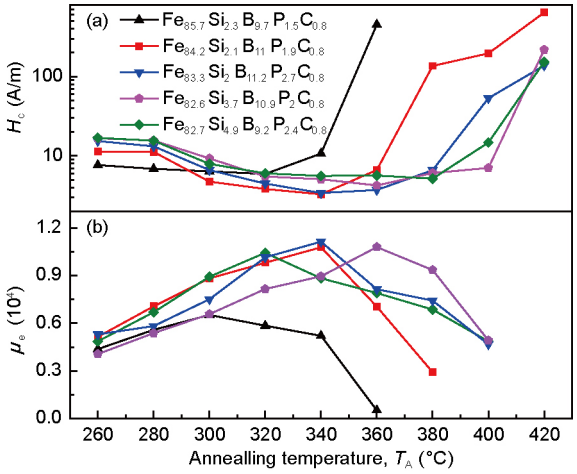

Figure 3 (Color online) Changes of coercive force (H_c) (a) and permeability (μ_e) (b) for the soft magnetic amorphous alloys as a function of T_A for 10 min.

amorphous alloys can be higher than 1×10^4 after annealing. Since the μ_e of the amorphous alloys is inversely proportional to H_c, the μ_e of the samples with extremely high H_c is not measured here. According to the XRD identification, the samples annealed at the optimal conditions exhibited fully amorphous microstructure.

As illustrated in Figure 4, these alloys annealed at the optimal annealing condition (annealing temperature with the lowest H_c) show the typical soft-magnetic *B*-*H* curves. The inset in Figure 4(a) depicts the enlarged partial curves of the *B*-*H* loops. Here the H_c is only 3.3-5.9 A/m. The B_s in Figure 4(b) of the soft magnetic amorphous alloys is in the range of 1.63-1.66 T. $Fe_{84.2}Si_{2.1}B_{11}P_{1.9}C_{0.8}$ (Fe-95 wt.%) amorphous alloy shows the highest B_s of 1.66 T, while for the $Fe_{85.7}Si_{2.3}B_{9.7}P_{1.5}C_{0.8}$ (Fe-95.5 wt.%) alloy, the B_s is only 1.63 T. The reason for non-monotonic increase of B_s with the rise of the Fe content is under further investigation and will be shown in our future work.

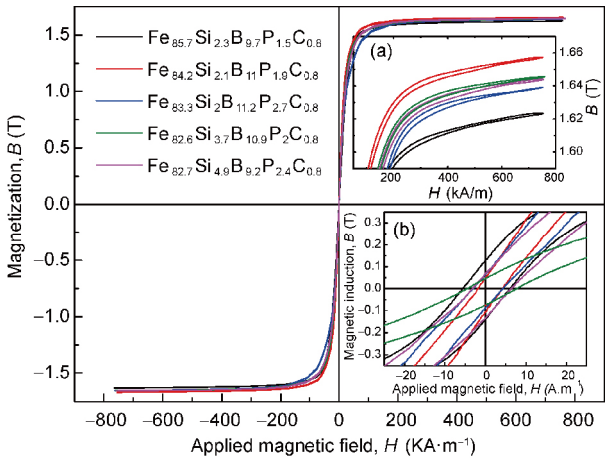

Figure 4 (Color online) (a) Hysteresis loops measured with VSM; (b) *B-H* loops measured with *B-H* loop tracer.

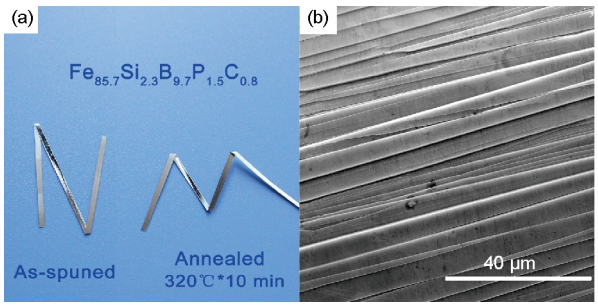

Figure 5 (Color online) (a) The $Fe_{85.7}Si_{2.3}B_{9.7}P_{1.5}C_{0.8}$ amorphous alloys after bending at 180°; (b) SEM image of shear zone in the bending region.

According to the bending test results of the annealed samples, the present alloys exhibit better bending ductility than commonly used $Fe_{78}Si_9B_{13}$ and $Fe_{82}Si_4B_{13}C_1$ alloy [21]. Here, we take as an example $Fe_{85.7}Si_{2.3}B_{9.7}P_{1.5}C_{0.8}$ (Fe-95.5 wt.%) alloy ribbon with the highest Fe content. As observed in Figure 5(a), there is no trace of any fracture for the as-spuned and annealed ribbons bended into 180°. After bending test, SEM image, which revealing the surface morphology of the annealed ribbon sample, was shown in Figure 5(b). A number of slip bands without shear offset can be seen in the vicinity of the bending region. The bending experiments demonstrate that the alloys show good bending ductility, even in the annealed state. The good bending ductility is vital for Fe-based amorphous ribbons for using as magnetic cores, which allows them to be easily wound into various cores in electrical magnetic devices.

For further understanding the excellent soft-magnetic properties, magnetic domains of the representative $Fe_{84.2}Si_{2.1}B_{11}P_{1.9}C_{0.8}$ (Fe-95 wt.%) ribbon sample annealed at 320°C were studied under different magnetic fields with Magneto-optical Kerr Microscopy. As shown in Figure 6(a), two typical domain patterns are found on the whole ribbon surface: (1) a low proportion of stripe-wide domain close to the edge with preferred orientation nearly perpendicular to the ribbon axis (enlarged in Figure 6(c)), (2) a dominated zigzag domain with a smaller width in the middle (enlarged in Figure 6(f)) [22]. No complex domain patterns like fine, curved, complex, maze domains can be seen in the whole surface of the sample, implying the thorough release of cast-in stress without crystals nucleating and surface crystallization. It is accepted that domain structures are the result of a complicated energy balance between magnetostatic stray field energies, anisotropic magnetic energy terms, and the exchange energy usually contained in the domain wall energy. According to the previous reports, the amorphous ribbon exhibits perpendicular magnetic anisotropy and the stripe domains can be interpreted as model in Figure 6(b) [23]. The magnetization directions are roughly perpendicular to the stripe and antiparallel for the neighboring domains. Thus the stripe and zigzag domains are closure domains. The domains are classified into bulk domains with perpendicular magnetization and closure domains at the surface. The closure domains are subclassified into stripe wide domain and zigzag domains. Since the domain wall energy $\gamma_B \propto D_0^{-2}$, where γ_B corresponds to specific wall energy and D_0 corresponds to domain wall width [24]. The rotation of magnetization direction in the zigzag domain in the middle will also lead to better closure and reduce anisotropy energy. In order to deeply investigate the domain model and magnetization process, the transition process of the two domains are observed by applying an increasing external magnetic field (H) with direction along the ribbon and perpendicular to the stripe. As shown in Figure 6(d), when H is smaller than the full magnetization field (H_1) of the closure domains, the width of the dark stripe domain with antiparallel direction decreases and the shallow one increases. When H increases to 796 A/m, the widths of both dark and shallow stripe in Figure 6(e) decrease, implying H_1 is smaller than 796 A/m. For the pictures (not listed) taken under $H \geq 1590$ A/m, no contrast can be detected. For the zigzag domain, more complicated transition is induced in Figure 6(g), suggesting the closure domain phagocytic growth and direction rotation. For the sample under 796 A/m, a regular stripe domain is formed from the zigzag domain. The magnetization process of the two types of domain sufficiently manifests the domain model we proposed in Figure 6(b).

In this work, we concentrate on amorphous alloys with distinctly higher Fe content than the traditional one. By introducing P and C, $Fe_{82.7\text{-}85.7}Si_{2\text{-}4.9}B_{9.2\text{-}11.2}P_{1.5\text{-}2.7}C_{0.8}$ amorphous alloys with excellent soft magnetic properties were successively developed. We propose it an effective breakthrough for the future development and application of amorphous alloys with Fe content in comparison with that of the desired high Si alloy. Here, we will try to explore the origin of good GFA, bending toughness, surface quality and excellent soft magnetic properties, which are always accompanied by a large

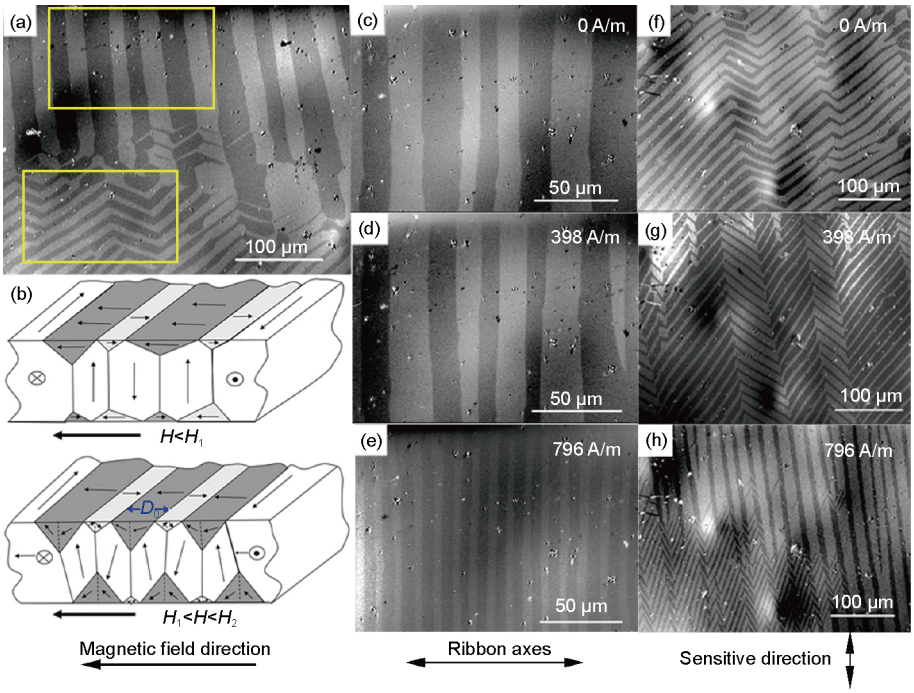

Figure 6 (Color online) Magnetic domain structure of $Fe_{84.2}Si_{2.1}B_{11}P_{1.9}C_{0.8}$ (Fe-95 wt.%) alloy ribbon annealed at 320°C for 10 min. (a) Domain image showing the representative patterns; (b) schematic domain model with their closure structure showing the magnetization process; (c)-(e) magnetization process of stripe domain at 0, 398, 796 A/m; (f)-(h) magnetization process of zigzag domain at 0, 398, 796 A/m.

amount of amorphous forming element addition. Multicomponent systems consisting of five elements in this alloy system is easier to form amorphous according to traditional experience [25], thus it is conducive to the increase of Fe content limitation. Metallic elements C and B have many differences in atomic size ratios with Fe element, which can help to form a compact structure. As B and C show lower relative atomic mass, it also can increase Fe content than other elements. In addition, Si, B, P and C have big negative mixing enthalpies with Fe, the appropriately addition significantly increases the thermal stability and GFA [26]. The good soft magnetic properties of the high Fe content amorphous alloys are mainly attributed to the high degree of amorphicity [27]. An important feature of amorphous alloys is, furthermore, the absence of any grain or phase boundaries which are known to act as strong pinning centers for domain walls in crystalline materials [28]. As another main pinning source, the internal stress derived from the fast cooling process is effectively relieved.

As the commercial $Fe_{78}Si_9B_{13}$ alloy exhibits a ductile-brittle transition between 250°C and 275°C, it is meaningful that the high Fe content amorphous alloys show good ductility even after annealing [29]. As a long standing problem for Fe-base amorphous alloys, the annealing induced embrittlement is usually attributed to BCC-type clusters, free volume annihilation, phase separation, and localized enrichment of highly diffusive elements like P, B, C and Si [21]. For these high Fe content alloys, low annealing temperatures would be enough for improving the soft magnetic property because low T_c, will lead to smaller microstructure changes. The good bending ductility is significant for the application of Fe-based amorphous ribbons in magnetic cores, which allows them to be easily wound into various cores in different devices.

4 Conclusions

$Fe_{82.7\text{-}85.7}Si_{2\text{-}4.9}B_{9.2\text{-}11.2}P_{1.5\text{-}2.7}C_{0.8}$ soft magnetic amorphous alloys with high Fe content, good manufacturability, excellent magnetic and mechanic properties were developed via component design and composition adjustment. The main conclusions are: (1) these alloys exhibit high Fe content 93.5-95.5 wt.% comparable with that of the desired high Si. (2) The ribbon samples exhibit excellent soft-magnetic properties after annealing, i.e., H_c of 3.3-5.9 A/m, μ_e of 5000-10000 and B_s in the range of 1.63-1.66 T. (3) Two typical domain patterns were identified by using Magneto-optical Kerr Microscopy. Low proportion of wide stripe domain locates close to the edge with preferred orientation nearly perpendicular to the ribbon axis, dominated zigzag domain shows smaller width. (4) The high Fe content amorphous alloys show good ductility even after annealing, which allows them to be easily wound into various cores in different devices. The good soft magnetic properties and ductility are important for the practical application.

This work was supported by the National Natural Science Foundation of China (Grant No. 51541106), Ningbo International Cooperation Projects (Grant No. 2015D10022), Ningbo Major Project for Science and Technology

(Grant No. 201401B1003003), Ningbo Natural Science Foundations (Grant No. 2015A610007), and General Research Fund of Hong Kong (Grant No. CityU 102013).

1 T. Kubota, M. Fujikura, and Y. Ushigami, J. Magn. Magn. Mater. **215-216**, 69 (2000).
2 T. Ros-Yañez, Y. Houbaert, and V. Gómez Rodŕiguez, J. Appl. Phys. **91**, 7857 (2002).
3 J. H. Yu, J. S. Shin, J. S. Bae, Z. H. Lee, T. D. Lee, H. M. Lee, and E. J. Lavernia, Mater. Sci. Eng. A **307**, 29 (2001).
4 H. Haiji, K. Okada, T. Hiratani, M. Abe, and M. Ninomiya, J. Magn. Magn. Mater. **160**, 109 (1996).
5 H. T. Liu, H. Z. Li, H. L. Li, F. Gao, G. H. Liu, Z. H. Luo, F. Q. Zhang, S. L. Chen, G. M. Cao, Z. Y. Liu, and G. D. Wang, J. Magn. Magn. Mater. **65**, 391 (2015).
6 Z. W. Zhang, W. H. Wang, Y. Zou, I. Baker, D. Chen, and Y. F. Liang, J. Alloys Compd. **639**, 40 (2015).
7 A. Inoue, Y. Shinohara, and J. S. Gook, Mater. Trans. JIM **36**, 1427 (1995).
8 X. Wang, W. Zhang, Z. Liu, H. Li, and G. Wang, Mater. Charact. **122**, 206 (2016).
9 K. Mohri, and S. Korekoda, IEEE Trans. Magn. **14**, 1071 (1978).
10 A. Inoue, A. Makino, and T. Mizushima, J. Magn. Magn. Mater. **215-216**, 246 (2000).
11 Z. B. Jiao, H. X. Li, Y. Wu, J. E. Gao, S. L. Wang, S. Yi, and Z. P. Lu, Sci. China-Phys. Mech. Astron. **53**, 430 (2010).
12 C. Chang, C. Qin, A. Makino, and A. Inoue, J. Alloys Compd. **533**, 67 (2012).
13 K. Suzuki, A. Makino, N. Kataoka, A. Inoue, and T. Masumoto, Mater. Trans. JIM **32**, 93 (1991).
14 A. Wang, C. Zhao, H. Men, A. He, C. Chang, X. Wang, and R. W. Li, J. Alloys Compd. **630**, 209 (2015).
15 M. Ohta, and Y. Yoshizawa, Mater. Jpn. **48**, 126 (2009).
16 C. Chang, T. Kubota, A. Makino, and A. Inoue, J. Alloys Compd. **473**, 368 (2009).
17 E. P. Barth, F. Spaepen, R. Bye, and S. K. Das, Acta Mater. **45**, 423 (1997).
18 C. Zhao, A. Wang, A. He, S. Yue, C. Chang, X. Wang, and R. W. Li, J. Alloys Compd. **659**, 193 (2016).
19 A. Wang, C. Zhao, A. He, H. Men, C. Chang, and X. Wang, J. Alloys Compd. **656**, 729 (2016).
20 P. Jalali, and M. Li, Intermetallics **12**, 1167 (2004).
21 G. Kumar, M. Ohnuma, T. Furubayashi, T. Ohkubo, and K. Hono, J. Non-Crystal. Solids **354**, 882 (2008).
22 R. Sahingoz, M. Erol, and M. R. J. Gibbs, J. Magn. Magn. Mater. **271**, 74 (2004).
23 G. Herzer, and H. R. Hilzinger, J. Magn. Magn. Mater. **62**, 143 (1986).
24 H. Kronmuller, M. Fahnle, M. Domann, H. Grimm, R. Grimm, and B. Groger, J. Magn. Magn. Mater. **13**, 53 (1979).
25 A. Inoue, A. Makino, and T. Mizushima, J. Magn. Magn. Mater. **215-216**, 246 (2000).
26 W. K. An, D. W. Ding, A. H. Cai, G. J. Zhou, Y. Luo, J. H. Li, and Y. Y. Peng, Sci. China-Phys. Mech. Astron. **58**, 066101 (2015).
27 Z. P. Chen, J. E. Gao, Y. Wu, H. Wang, X. J. Liu, and Z. P. Lu, Sci. China-Phys. Mech. Astron. **57**, 122 (2014).
28 T. Bitoh, A. Makino, and A. Inoue, Mater. Trans. **44**, 2020 (2003).
29 Y. C. Niu, X. F. Bian, and W. M. Wang, J. Non-Crystal. Solids **341**, 40 (2004).